# A NOVEL QUALITY FACTOR FOR THERMOPLASTIC COMPOSITES WELDING

### A. Sänger\*

\* Center for Lightweight Production Technology, German Aerospace Center (DLR), Am Technologiezentrum 4, 86159 Augsburg, Germany

#### **Abstract**

Fibre-reinforced thermoplastics are increasingly replacing metal alloys in aerospace due to their low weight, high specific strength and possibility to be welded. However, traditional development processes for joining technologies are experimentally based hence resource-intensive. This work introduces a novel thermally based quality factor, the Sänger factor, to predict the mechanical joint strength of resistance-welded thermoplastic composites using simulated temperature data. The approach leverages a meso-scale model, the newly modified mosaic model ( $M^3$ ) to capture heterogeneous heating patterns and integrates four temperature characteristics: degree of melting, degradation, homogeneity, and crystallisation potential. The model was validated experimentally using single lap shear tests and evaluated across various process configurations. Results demonstrate a strong correlation between thermal and mechanical properties, with prediction accuracies exceeding 90 % for a  $\pm$  10 % error margin and 75 % for the  $\pm$ 2 $\sigma$  confidence interval. Thereby, the Sänger factor offers a digital, resource-efficient method to optimise thermoplastic joining processes and reduce experimental effort.

### Keywords

Fibre-reinforced Thermoplastic; Resistance Welding; Quality Prediction

#### 1. INTRODUCTION

### 1.1. Background

Fibre composite materials, with their low weight and high specific strength, are increasingly replacing conventional metal alloys to reduce aircraft weight [1, p. 33].

Currently, thermosetting matrix materials dominate aerospace applications despite their ecological drawbacks, such as energy-intensive storage and autoclave curing processes, high resource consumption for auxiliary materials, and difficulties in recycling components [2, 3]. Additionally, time-consuming manual steps have a negative impact as well as slow reaction times [4,5].

Thermoplastics are emerging as a promising material in aerospace due to their advantages over thermosetting processes. The elimination of auxiliary materials and slow curing processes makes thermoplastic welding faster and more cost-effective, allowing for a high degree of automation [6–8]. In addition, dust- and chip-free welding is particularly interesting as it can streamline the currently serial production chain, enabling parallelisation through pre-assembled sub-components [3, 9].

Thermoplastics have thus become a key matrix system in fibre composites, enabling the exploration of new joining technologies [6–8, 10, 11].

## 1.2. State of the Art

The standard approach for developing new joining processes involves the production of experimental samples followed by mechanical tests [6, 11, 12] following a test pyramid scheme [13]. This requires numerous sequential tests, making it resource-intensive in terms of time, cost, and materials [14]. Alternative materials and optimisation potentials are often overlooked, and scalability issues arise when increasing the joint length [15, 16].

Aerospace certification is based on empirical test results, providing rigid process windows that are difficult to adapt to changes such as material modifications [17]. Furthermore, current development processes lack a comprehensive virtual process chain, prompting a shift towards digital aircraft development to reduce time, material use, costs, and risks [18–22]. This trend is supported by the European Union Aviation Safety Agency (EASA), which has outlined requirements for modelling and simulation in future certification processes [23].

Numerical models and process simulations are increasingly used in developing new joining technologies for thermoplastic composites, particularly for induction, ultrasonic, and resistance welding [6, 8, 11, 24]. Recent advancements in finite element modelling (FEM) have enabled process simulations for induction and ultrasonic welding [25–29]. Resistance welding has seen previous numerical approaches, with various studies focussing on temperature distribution and optimisation of process parameters [14, 30–37].

Quality prediction based on process simulations is increasingly emphasised, with some studies identifying optimal process windows through FEM simulations [14, 32, 38, 39]. However, dedicated quality prediction efforts are primarily seen in ultrasonic welding [40–45].

## 1.3. Motivation

In contrast to the traditional form-fit joining of conventional metallic aircraft structures, thermoplastic welding creates a material bond significantly influenced by the manufacturing process [46]. To infer the quality of the joint produced, the process must be comprehensively understood and analysed [47, pp. 65]. Previous studies have established that the quality and strength of the joint are directly related to the thermal history in the joining zone [32]. Additionally, a correlation has been found between process temperatures

and the resulting joint area, to which mechanical strength is proportional [37].

Currently, the development of process simulations and predictive models occurs separately [43, 48]. This work addresses the identified gap between process simulation and quality prediction based on the investigation of the temperature in the joining zone as a key characteristic. It thus contributes to shorter development times with reduced resource consumption while simultaneously increasing the degree of digitalisation in the research of new joining technologies. In addition, it offers easy applicability for numerous welding processes of thermoplastic fibre composites.

### 2. METHODOLOGY

#### 2.1. Process and Materials

As subject of investigation, this work focuses on electrical resistance welding, which utilises the physical phenomenon of heating a conductive element placed between the joining partners (Figure 1).

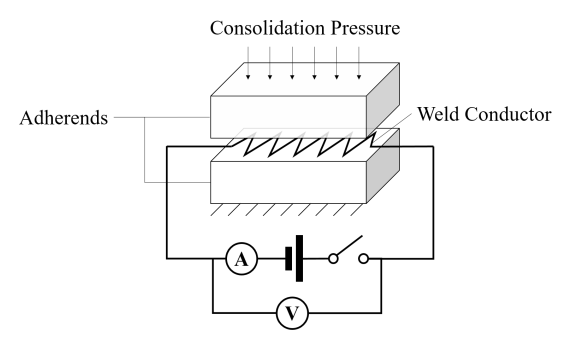


FIG 1. Schematic Setup

When a direct current is applied and the supplied energy exceeds thermal losses to the surroundings, the temperature of the weld conductor and adjacent layers rises until the melting range of the thermoplastic matrix is reached. Once sufficient surface melting is achieved, the current is discontinued, and the joint cools under an appropriate consolidation pressure, ensuring good contact and adequate molecular diffusion in the joining zone.

Table 1 lists the four investigation groups which are defined in order to assess the later introduced quality prediction: the baseline configuration (I) and its up-scaled process (II) as well as transferability to different pressure piece materials (III) and matrix systems (IV).

**TAB 1. Overview of Investigation Groups** 

Group	Matrix	Weaving	Pressure Piece	Joint Area [mm x mm]
ı	PPS	5HS	Invar 36	200 x 40
Ш	PPS	5HS	Invar 36	600 x 38
III	PPS	5HS	Ceramics	200 x 40
IV	LMPAEK	UD*	Ceramics	200 x 25

\*Weld Conductor: Toray CETEX® TC1225, T300JB, 277 gsm

Adherends consist of pre-consolidated, five-harness satin (5HS) polyphenylenesulfide (CF/PPS) woven prepregs (Toray CETEX® TC1100, T300JB, 280 gsm) in five layer configuration ([ $\pm$ 45, 0/90,  $\pm$ 45, 0/90,  $\pm$ 45]). Additionally, experiments with twelve unidirectional layers ([45, 0, -45, 0, 90, 0]<sub>S</sub>) low-melt polyaryletherketone

(CF/LMPAEK) manufactured via automated fibre placement (AFP) are carried out. All weld conductors are single-layer 5HS woven fabrics ([0/90]) of the respective adherend matrix system. Between current carrying weld conductor and adherends, an electrically isolating EC5 glass fibre fabric (2/2 twill) is inserted on either side. Consolidation pressure is applied by pressure pieces either from VDM® Invar 36 with integrated heating cartridges HS-86/100/230 or KTherm® AS700 ceramics without heating. Within the groups, the five key performance parameters pressure piece temperature, consolidation pressure, heating voltage, heating duration and holding voltage are varied to establish in total 29 process variants.

### 2.2. Modelling

Literature on welding process modelling of thermoplastic composites predominantly employs macroscopic approaches with homogenised layers [49, 50]. However, these methods sacrifice critical microscopic physical interactions, thereby predictive accuracy for computational efficiency [49–51].

Thermal history and temperature distribution critically influence joint quality, with inhomogeneous heating caused by the composite's heterogeneous structure [32, 37, 52–55]. Microscopic and thermographic images reveal heterogeneous heating patterns in carbon fibre weld conductors due to anisotropic electrical resistance (Figure 2, top/middle), which cannot be described by macroscopic approaches (Figure 2, bottom).

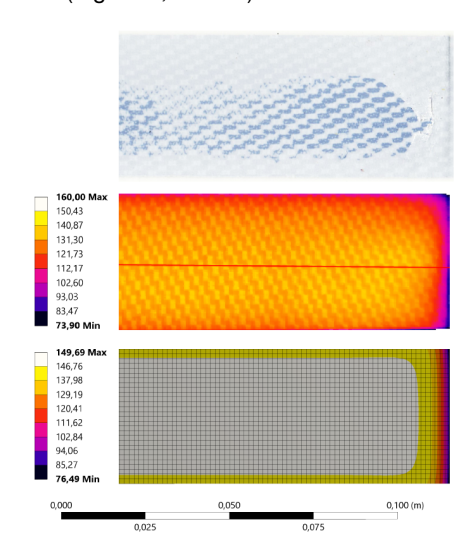


FIG 2. Microscopic image (top), thermographic image (middle, [56]) and simulated temperatures of a macroscopically modelled weld conductor (bottom)

To capture these fundamental heating effects, a meso-scale model – resolving at least the roving level – is essential. The mosaic model by Ishikawa [57–60] was originally developed for purely mechanical behaviour of textile fabrics, but balances accuracy and computational efficiency, resolving fibre-level details while maintaining manageable complexity. For thermal-electric modelling, the mosaic model is adapted to include contact surfaces between elements, classified as interplanar (IP), interfilament (IF), and resin wedge (HK) with assigned thermal  $(\tau)$  and electrical  $(\varepsilon)$  contact coefficients to simulate heat and current flow; fibre continuity is ensured by loss-free node coupling. Thereby, the modified mosaic model ( $\mathrm{M}^3$ , Figure 3) is introduced which is implemented in Ansys 2020 R1 via custom and parametrised APDL scripts which can easily be adjusted to different fibre architectures.

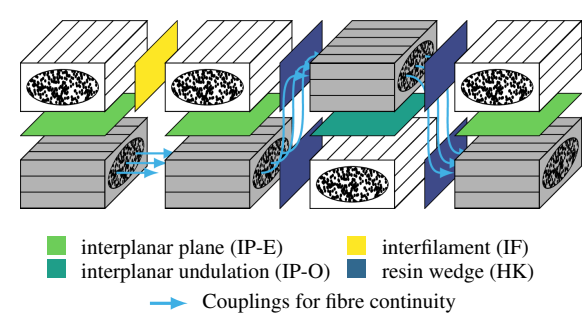


FIG 3. Modified Mosaic Model (M3)

### 2.3. Mechanical Characteristics

The most common method for characterising the strength of resistance-welded joints is the single lap shear test (SLS), which yields the lap shear strength (LSS), denoted as  $\tau_{\scriptscriptstyle W}$  [24]. It can be compared to the base material strength,  $\tau_{\scriptscriptstyle \infty}$ , representing the maximum possible joint strength. This reference value is determined using fully consolidated plates manufactured in a hot press and tested with the same lap shear method [61].

The mechanical weld factor,  $\Theta_M$ , is calculated as the ratio of these two values according to

(1) 
$$\mathscr{F}_{Mech}( au)$$
 :  $\Theta_M = \frac{ au_W}{ au_\infty}$ , where  $\Theta_M \in [0,1]$ .

This ratio is widely used in the literature to assess the degree of consolidation [16,35,61] and will also be employed in this work to evaluate the mechanical quality of the joint. An optimal weld strength is indicated by  $\Theta_M=1$ .

For this work, all mechanical values are determined according to DIN EN 2243-1 [62] at room temperature (23 °C) with a Zwick BZ1-MM14780.ZW01 tensile testing machine. Only tested specimens with an interlaminar failure mode [63] as well as a relative standard deviation of the mean value of less than ten percent are considered.

### 2.4. Hypothesis on Mechanical-Thermal Analogy

Numerous studies have established a direct correlation between mechanical joint strength and the thermal history within the joining zone [15, 32, 52, 53], with joint quality proportional to process temperatures and the generated bonding area [37]. This work hypothesises the existence of a thermally based quality factor,  $\mathscr{F}_{\text{Sänger}}$ , derived solely from the temperature state at the end of the heating or consolidation phase. This factor is posited to be equivalent to the mechanical weld factor,  $\mathscr{F}_{\text{Mech}}$ , such that

$$(2) \qquad \mathscr{F}_{S\"{a}nger}(\vartheta) \equiv \mathscr{F}_{Mech}(\tau), \quad \text{where} \quad \mathscr{F}_{S\"{a}nger} \in [0,1]\,.$$

Proving this hypothesis would enable the characterisation and prediction of mechanical joint strength using only simulated temperature data, eliminating the need for further mechanical tests.

## 2.5. Mathematical Approach

Machine learning has demonstrated effectiveness in solving material and engineering challenges [64], including quality prediction in ultrasonic welding of thermoplastic composites [41, 43–45]. This work adapts supervised learning principles, focusing on manual parameter optimisation. The goal is to map input temperature characteristics to the continuous output of the mechanical weld factor,  $\mathscr{F}_{\text{Mech}}(\tau)$ ,

using a linear regression model which assumes a hypothesis function of the form

(3) 
$$h_{\theta}(x) = \theta_0 + \theta_1 \cdot x_1 + \ldots + \theta_n \cdot x_n$$

where  $\theta_i$  are weighting factors and  $x_i$  are known regressors.  $\theta_0$  is a random unknown noise of additional hidden variables. For this term, the convention should be introduced that  $x_0 = 1$  always applies, whereby (3) can be rewritten as

(4) 
$$h_{\theta}(x) = \langle \theta | x \rangle = \sum_{i=0}^{n} \theta_{i} \cdot x_{i}.$$

### 2.6. Temperature Characteristics

The regressors,  $x_i$ , are selected to represent the temperature state's influence on joint quality. Four key characteristics are identified.

## 2.6.1. Degree of Melting $\Psi_m$

The degree of melting,  $\Psi_m$ , indicates whether the required melting temperature,  $T_m$ , is reached during heating. Temperatures below  $T_m$  prevent bonding, as confirmed by [15, 39, 52]. This temperature level also influences subsequent consolidation and crystallisation defining the lower bound of the optimal process window [32, 34, 65].

"Unlike metals, [...] semicrystalline polymers melt over a relatively broad range." [66, p. 11] This behaviour arises due to the inhomogeneous distribution of amorphous and crystalline regions, which begin to melt at different times around the crystalline melting temperature,  $T_m$  [67, pp. 86]. Consequently, a continuous method – rather than a discrete, melting-point-based approach – is selected to model the melting behaviour. Experimentally, this is typically characterised using differential scanning calorimetry (DSC) measurements [68, pp. 160].

Thereby, the specific enthalpy of fusion  $\Delta h_m$  is represented by the area between the DSC curve and the baseline between onset and endset temperature points  $T_{on}$  and  $T_{end}$ , respectively, i. e. the integral

(5) 
$$\Delta h_m = \int_{t}^{t_{end}} \left[ \left( \frac{dq}{dt} \right)_{specimen} - \left( \frac{dq}{dt} \right)_{baseline} \right] dt,$$

with the different points of time  $t_{on}$  and  $t_{end}$ , respectively, exhibiting onset and endset temperature.

For incomplete melting up to a temperature  $\vartheta$  between  $T_{on}$  and  $T_{end}$ , the melting enthalpy expended up to that point,  $\Delta h_m(\vartheta)$ , is calculated using the integral function

(6) 
$$\Delta h_m(\vartheta) = \int_{t}^{t_{\vartheta}} \left[ \left( \frac{dq}{dt} \right)_{specimen} - \left( \frac{dq}{dt} \right)_{baseline} \right] dt.$$

The experimental degree of melting,  $\Psi_m^{DSC}$ , for incomplete melting between the onset and endset temperatures,  $T_{on}$  and  $T_{end}$ , is determined by the ratio of the heat flow expended up to that point to the total melting enthalpy, as per

(7) 
$$\Psi_m^{DSC}(\vartheta) = \frac{\overline{\Delta h_m}(\vartheta)}{\overline{\Delta h_m}}$$
 for  $T_{on} \le \vartheta \le T_{end}$ .

For simplicity, it is assumed that no melting occurs below the onset temperature,  $T_{on}$  ( $\Psi_m = 0$ ), and that the laminate is fully molten above the endset temperature,  $T_{end}$  ( $\Psi_m = 1$ ).

©2025

3

Consequently, the degree of melting,  $\Psi_m$ , is defined as

$$(8) \quad \Psi_m(\vartheta) = \left\{ \begin{array}{lll} 0 & \text{for} & \vartheta < T_{on}, \\ \Psi_m^{DSC}(\vartheta) & \text{for} & T_{on} \leq \vartheta \leq T_{end}, \\ 1 & \text{for} & \vartheta > T_{end}. \end{array} \right.$$

Figure 4 shows schematically the DSC melting curve (exemplary for Cetex® TC1110 CF/PPS laminate) with the hatched area representing the enthalpy of fusion  $\Delta h_m$  (top) and the corresponding degree of melting  $\Psi_m$  (bottom) according to Equation 8.

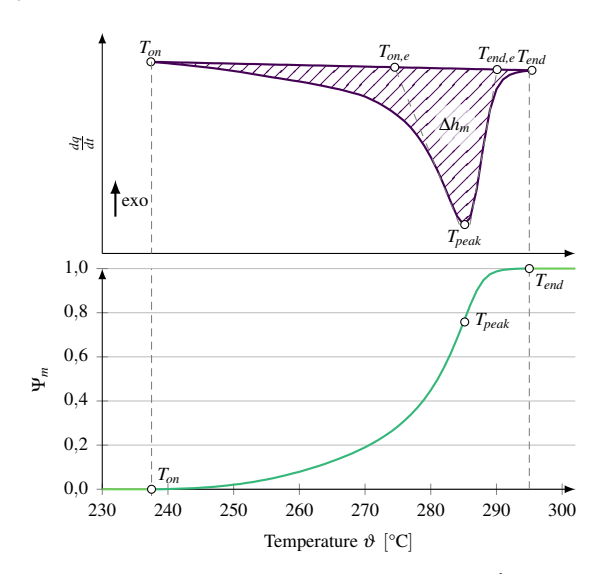


FIG 4. Schematic DSC melting curve (heat flow  $\frac{dq}{dt}$ , top) and corresponding Degree of Melting  $\Psi_m$  (bottom)

## 2.6.2. Degree of Degradation $\Psi_d$

Process temperatures must not exceed the degradation temperature,  $T_d$ , during heating, as surpassing this threshold irreversibly damages polymer bonds and reduces mechanical properties of the polymer [69, 70, pp. 68,18] as well as of the joint [35,65].

Similar to [65], discrete modelling approach is adopted to distinguish temperatures above and below the degradation temperature,  $T_d$ . Therefore, the degradation temperature is determined by thermogravimetric analysis (TGA) and is derived as the temperature where the inflection point of the remaining mass fraction curve occurs. The degradation degree,  $\Psi_d$ , is defined in its *complementary form* as per

(9) 
$$\Psi_d(\vartheta) = \left\{ \begin{array}{lll} 1 & \text{ for } & \vartheta & < & T_d, \\ 0 & \text{ for } & \vartheta & \geq & T_d, \end{array} \right.$$

since maximum degradation corresponds to minimal strength in quality assessment.

Figure 5 shows schematically the TGA remaining mass fraction curve (exemplary for Cetex® TC1110 CF/PPS laminate, top) and the corresponding degree of degradation  $\Psi_d$  (bottom) according to Equation 9.

# 2.6.3. Homogeneity of Temperature Distribution $\Psi_h$

Temperature distribution across the joining area is often inhomogeneous due to material, process, and external factors, potentially creating both molten and unmelted regions. Such gradients increase the risk of voids and air inclusions, which degrade mechanical properties by altering fibre volume content and promoting crack initiation [71, pp. 1]. Liter-

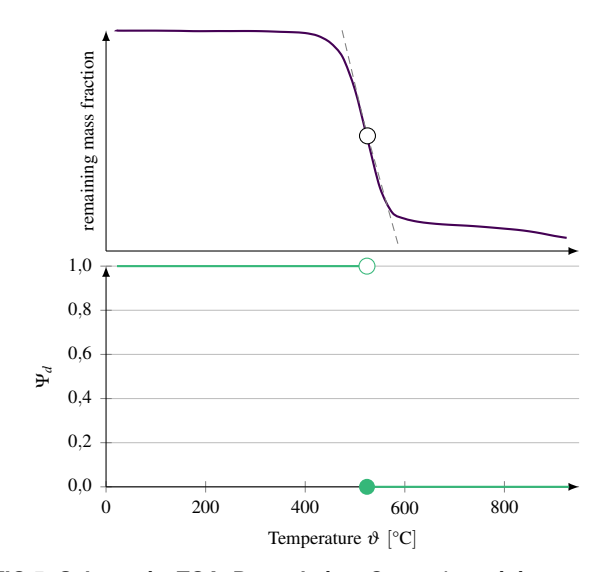


FIG 5. Schematic TGA Degradation Curve (remaining mass fraction, top) and corresponding Degree of Degradation  $\Psi_d$  (bottom)

ature confirms that uneven temperature distribution reduces joint quality, with edge areas often exhibiting poorer bonding and increased porosity [15, 16, 52, 53, 72, 73].

There are no preliminary studies in the literature on quantifying the homogeneity of temperature distributions. Instead, in automated image processing, an image is considered homogeneous if every pixel has the same colour, and homogeneity is quantified using the standard deviation, s, of each pixel's greyscale value relative to the mean greyscale value of the image [74]. Applied to the distribution of simulated element temperatures,  $\vartheta_i$ , this yields

(10) 
$$s(\vartheta_i) = \sqrt{\frac{1}{n-1} \sum_{i=1}^{n} \left(\vartheta_i - \overline{\Delta} \vartheta\right)^2}.$$

with the arithmetic mean value of the element temperatures  $\overline{\vartheta_i}$  normalised to the peak melting temperature,  $T_{peak}$ , determined from DSC measurements, following

(11) 
$$\overline{\Delta\vartheta} = \frac{1}{n} \sum_{i=1}^{n} \left( \vartheta_i - T_{peak} \right),$$

Since the standard deviation can be of any value, but the degree of homogeneity shall obey  $\Psi_h \in [0,1]$ , a standardisation is introduced analogous to [75], which sets the standard deviation in relation to the mean temperature as

$$\text{(12)} \quad \Psi_h(\vartheta) = \left\{ \begin{array}{cccc} 1 - \frac{s(\Delta\vartheta_i)}{\Delta\vartheta} & & \text{for} & & s(\Delta\vartheta_i) & < & \overline{\Delta\vartheta}, \\ 0 & & \text{for} & & s(\Delta\vartheta_i) & \geq & \overline{\Delta\vartheta}. \end{array} \right.$$

## 2.6.4. Crystallisation Potential $\Psi_c$

4

Unlike previous thermal factors, the crystallisation degree does not only assess a certain point in time but characterises the cooling behaviour during consolidation, directly impacting joint quality [76–78]. High temperature gradients influence matrix crystallisation, with slower cooling rates increasing crystallinity and enhancing mechanical properties, such as elastic modulus and tensile strength [67, 79, pp. 291,86]. Numerical studies on resistance welding and consolidation processes frequently incorporate crystallisation behaviour [30,31,80–82].

©2025

Absolute crystallinity,  $\chi_a$ , reflects the extent of crystalline regions, but consistently remains below the maximum possible crystallinity levels of about 50-65% [83], which does not align with the specified value range for the novel quality factor in Equation 2 as  $\Psi_c \in [0,1]$ . By contrast, relative crystallinity,  $\chi_r$ , describes the progression of crystallisation relative to the final state and ranges from 0 to 1, but does not reflect the final crystallinity achieved.

To address this, a new metric, *crystallisation potential*,  $\Psi_c$ , is defined as the ratio of generated absolute crystallinity to the initial crystallinity of the base materials following

(13) 
$$\Psi_c = \frac{\hat{\chi}_a}{\chi_a^{ini}}.$$

This assumes that a joint is of high quality if its crystallinity closely matches that of the original semi-finished products. The combined absolute crystallinity,  $\hat{\chi}_a$ , accounts for both molten and unmelted regions using a weighted average

(14) 
$$\hat{\chi}_a = \zeta_{\gamma} \cdot \chi_a + (1 - \zeta_{\gamma}) \cdot \chi_a^{ini},$$

where  $\zeta_{\chi}$  is the ratio of molten to unmelted areas.

The absolute crystallinity,  $\chi_a$ , in molten regions is estimated using the Modified Nakamura-Ziabicki (MNZ) model, which can be adapted to absolute crystallinity using [84], reading

(15) 
$$\chi_a = \int_{t_0}^{\tau} \mathcal{K}(T, \dot{T}) \cdot \mathcal{G}(\chi_a) dt,$$

with the functions  $\mathscr{G}(\chi_a,\chi_a^{ini})$  and  $\mathscr{K}(T,\dot{T})$  according to

(16a)

$$\begin{split} \mathscr{G}(\chi_a,\chi_a^{ini}) &= \chi_a \cdot n \cdot \left(1 - \frac{\chi_a}{\chi_a^{ini}}\right) \cdot \left[ -\ln\left(1 - \frac{\chi_a}{\chi_a^{ini}}\right) \right]^{1 - \frac{1}{n}}, \\ \text{(16b)} \quad \mathscr{K}(T,\dot{T}) &= \mathscr{K}_{max}(\dot{T}) \cdot e^{-\frac{4\ln 2(T - \mathscr{T}_{max}(\dot{T}))^2}{\mathscr{D}(\dot{T})^2}}, \end{split}$$

comprising the AVRAMI exponent n as well as the crystallisation kinetic parameters following approach functions with logarithmic and power-law regressions as per

(17a) 
$$\mathscr{K}_{max}(\dot{T}) = C_1 + C_2 \cdot \ln|\dot{T}|,$$

(17b) 
$$\mathscr{T}_{max}(\dot{T}) = C_3 \cdot |\dot{T}|^{C_4},$$

(17c) 
$$\mathscr{D}(\dot{T}) = C_5 \cdot |\dot{T}|^{C_6}.$$

All aforementioned material related constants are determined via curve fitting of DSC data [85, 86].

## 2.6.5. Edge-Area-Weighting

Experimental results demonstrated that the condition of the edge regions, particularly due to stress concentrations at the overlap ends, is characteristic of measurable joint strength, while load transfer through the central area was secondary. A correlation was also observed between the width of unconsolidated edge regions and the resulting failure loads [87]. Based on these findings, an edge region of width  $d_{Edge}$  is defined along each longitudinal side of the joining zone (Figure 6).

In turn, all temperature characteristics,  $\Psi_i$ , are quantified separately for edge,  $\psi_{i,R}$ , and central,  $\psi_{i,F}$ , regions and then combined using weighted addition to emphasise the dominant influence of the edge regions reading

(18) 
$$\Psi_i = \zeta_R \cdot \psi_{i,R} + (1 - \zeta_R) \cdot \psi_{i,F},$$

with the weighting factor  $\zeta_R$  of the edge area.

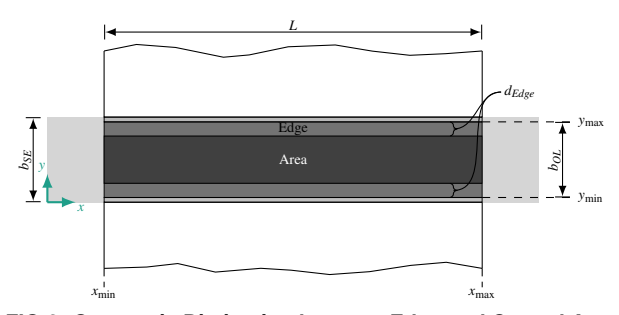


FIG 6. Geometric Distinction between Edge and Central Area

### 2.7. Formulation of the SÄNGER Factor

With the introduced temperature characteristics  $\Psi_i$ , the temperature-dependent quality factor  $\mathscr{F}_{\text{Sänger}}(\vartheta)$  can finally be postulated as the so-called Sänger factor  $\Theta_{\text{S}}$  as

(19) 
$$\mathscr{F}_{\text{Sänger}}(\vartheta)$$
 :  $\Theta_{S} = \langle \theta | \Psi \rangle = \begin{pmatrix} \theta_{0} \\ \theta_{m} \\ \theta_{d} \\ \theta_{h} \\ \theta_{c} \end{pmatrix} \cdot \begin{pmatrix} 1 \\ \Psi_{m}(\vartheta) \\ \Psi_{d}(\vartheta) \\ \Psi_{h}(\vartheta) \\ \Psi_{b}(\vartheta) \\ \Psi_{c}(\vartheta) \end{pmatrix}$ 

with weighting factors  $\theta_i$  satisfying

$$\sum_{i=0}^{n} \theta_i = 1.$$

### 3. RESULTS AND DISCUSSION

## 3.1. Model Quality Metrics

The optimal parameters,  $\hat{\theta}$ , are determined by minimising a loss function, such as the mean squared error (MSE),  $J_s$ , or mean absolute error (MAE),  $J_a$  respectively,

(21a) 
$$J_s(\theta) = \frac{1}{n} \sum_{i=1}^{n} [h_{\theta}(x) - y]^2,$$

(21b) 
$$J_a(\theta) = \frac{1}{n} \sum_{i=1}^{n} |h_{\theta}(x) - y|,$$

to ensure the closest fit between predicted and actual values,  $h_{\theta}(x)$  and y, respectively [88,89].

The mechanical weld factor,  $\Theta_M$ , from section 2.3 comes with a confidence interval,  $\Delta\Theta_M$ , which is defined as the standard deviation of the mean for a statistical confidence of  $p=95\,\%~(\pm\,2\sigma)$ . It can be directly compared with the mean absolute error (MAE) of the SÄNGER factor,  $\Theta_S$ . Thus, Equation 21b can be rewritten as

(22) 
$$J_a(\hat{\theta}) = \frac{1}{n} \sum_{i=1}^{n} \left| \Theta_S(\hat{\theta}) - \Theta_M \right|.$$

If  $J_a(\hat{\theta}) < \Delta \Theta_M$ , the simulated Sänger factor,  $\Theta_S$ , lies within the confidence interval of the experimentally determined joint strength (Figure 7), indicating that the thermal model sufficiently accurately represents the mechanical behaviour. Despite the typical  $\pm 2\sigma$  confidence interval, the validation criteria for modelling and simulation, as outlined by [23,90], specifies an acceptable error margin of  $\pm 10\,\%$  for derived quantities which shall be considered for assessment of the model quality, too.

©2025

5

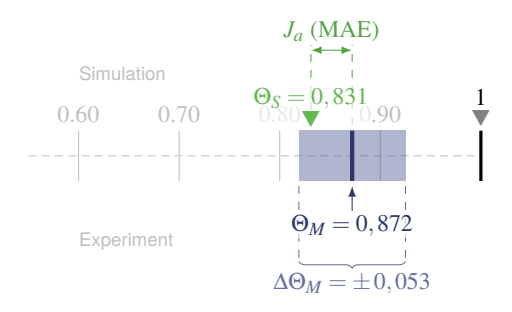


FIG 7. Exemplary relation between Mechanical Weld Factor,  $\Theta_M$ , and the computed SÄNGER factor,  $\Theta_S$ 

Therefore, the relative average error reads

(23) 
$$e = \left(\frac{\Theta_{\mathcal{S}}(\hat{\theta})}{\Theta_{\mathcal{M}}} - 1\right) \cdot 100 \%.$$

The results are also classified into binary categories using a confusion matrix (Table 2), where rows represent actual values and columns predicted values [91, pp. 201–202].

TAB 2. Generic Confusion Matrix

		Prediction			
		positive	negative	Σ	
Reality	positive	$t_p$	$f_n$	$t_p + f_n$	
	negative	$f_p$	$t_n$	$f_p + t_n$	
	Σ	$t_p + f_p$	$f_n + t_n$	n	

In this context, a "true positive"  $(t_p)$  corresponds to a valid correlation within the  $\pm$  10 % margin. Underestimating the actual strength by more than 10 % results in a "false negative"  $(f_n)$ , indicating a conservatively predicted quality, while overestimating it by more than 10 % yields a "false positive"  $(f_p)$ , indicating an optimistically predicted strength. The "true negative" category remains unassigned but does not affect subsequent metrics. The populated confusion matrix for evaluating the thermal model is shown in Table 3.

TAB 3. Confusion Matrix for the Thermal Model

		Prediction		
		positive negative		
Reality	positive negative	$ e  \leq 10\%$ progressive	conservative	

From these classes, three key performance metrics can be derived [88,89, pp. 13, 35–36]:

Accuracy reflects the proportion of correctly classified predictions (both positive and negative) relative to the total number of cases following

(24) 
$$acc = \frac{t_p + t_n}{t_p + f_p + t_n + f_n}.$$

Precision measures the proportion of true positive predictions among all positive predictions (both true and false) reading

$$prec = \frac{t_p}{t_p + f_p}.$$

Sensitivity, also called recall, represents the true positive rate, indicating the proportion of correctly predicted positive cases relative to all actual positive cases as

$$rec = \frac{t_p}{t_p + f_n}.$$

#### 3.2. Validation

The model development process begins with a grid search approach over the entire data set, a brute-force method used for hyper parameter optimisation in machine learning [92,93]. This method systematically explores all possible combinations within a defined solution space, though it is computationally intensive and suffers from the "curse of dimensionality" [94]. To mitigate this, a two-step process is employed with an initial coarse grid search identifying a promising region and setting the optimal edge distance  $(d_{Edge} = 5.716 \,\mathrm{mm})$ , followed by a finer search within that region. The latter refines the resolution of  $\zeta_R$  and  $\theta_i$  to increments of 0.001, focusing on the range around the initial optimum. This results in approximately 125 million configurations, with a typical runtime of 30 seconds. The mean squared error (MSE) and mean absolute error (MAE) are used as optimisation criteria.

The so determined optimised parameter set is used to evaluate the global correlation between thermal and mechanical properties across the entire dataset. The mean absolute deviation between  $\Theta_S$  and  $\Theta_M$  is approximately 0.2%, with individual deviations ranging from  $-7.6\,\%$  to + 11.2% nearly matching the allowable error margin of  $\pm$  10%. The standard deviation is  $\pm$  5.0%, indicating acceptable measurement uncertainty.

Of the 29 analysed datasets, 28 predictions (96.4%) fall within the  $\pm\,10\,\%$  error margin, and 23 (79.3%) lie within the  $\pm\,2\sigma$  confidence interval (Table 4). The model demonstrates high accuracy (96.6%/79.3%) and precision (96.6%/85.2%), with sensitivity exceeding 90% for both validation criteria,  $\pm\,10\,\%$  and  $\pm\,2\sigma$ . Thereby, the results confirm a strong correlation between thermal and mechanical properties.

TAB 4. Binary Quality Measure of the Global Correlation

	$\pm10\%$	$\pm2\sigma$
$true\ positive\ t_p$	28	23
false negative $f_n$	0	2
false positive $f_p$	1	4
Accuracy	96,6%	79,3%
Precision	96,6%	85,2%
Sensitivity	100%	92,0%
	•	

### 3.3. Extrapolation

6

This study initially used an interpolating scenario in the previous section, confirming the hypothesis of mechanical-thermal analogy using data within the validation set. The focus now shifts to evaluating the model's extrapolative capability for quality prediction.

For this purpose, k-fold cross-validation is employed since it mitigates high variances in model accuracy for small datasets [89,91,95]. The respective dataset is randomly divided into k subsets, with each subset used once as the test set and the remaining subsets for training. Typically, k=4

©2025

or 5 subsets are used, and the mean cross-validation error  $\overline{J_a}$  is computed as per

$$\overline{J_a} = \frac{1}{k} \sum_{i=1}^k J_{a,i}.$$

Three correlation groups are introduced to evaluate prediction quality, the corresponding computed results can be found in Table 5 and are discussed in the following.

### 3.3.1. General Correlation

The general correlation assesses the model's predictive quality and universality of the thermal model across all process configurations. The 29 valid datasets are randomly shuffled and divided into k=5 groups each containing five or six datasets. A 5-fold cross-validation is subsequently performed with the mean squared error (MSE) loss function,  $J_s$ , to be minimised.

For four of the five iterations, the prediction error is smaller than the experimental variation range, indicating high accuracy. The binary metrics show over 90 % accuracy and precision for the  $\pm\,10$ % error band and a 100 % recall rate. For the narrower  $\pm\,2\sigma$  confidence interval, the metrics remain robust, with an average accuracy and precision of 76% and 83%, respectively, and sensitivity exceeding 93%.

## 3.3.2. Special Correlation

The specific correlation investigates prediction quality within subgroups of similar process configurations. The analysis focuses on Groups I and II, which share nearly identical setups except for joint length.

Group I. The seven valid datasets are randomly divided into three groups each containing two or three datasets. The results show significant variations in weighting factors and prediction deviations. While one iteration achieves excellent accuracy (MAE = 0.006), others exhibit deviations up to 10 % above the experimental variation range which can be attributed to the limited number of datasets. Binary metrics indicate 100 % accuracy and precision for the  $\pm\,10$  % error band, but values drop to around 61 % accuracy and 78 % precision for the  $\pm\,2\sigma$  confidence interval.

*Group II.* The 16 valid datasets are divided equally into four groups. Three iterations show prediction deviations smaller than the experimental variation range, with one outlier at 20%. Generally, higher accuracy is achieved when baseline configurations are included in the training set. Binary metrics reveal high model quality, with over 90 % accuracy and precision for the  $\pm\,10\,\%$  error band and 75 % for the  $\pm\,2\sigma$  confidence interval.

Group I+II. Combining Groups I and II, the 23 valid datasets are divided into four groups each containing five or six datasets. All iterations show prediction deviations below the experimental uncertainty range. Binary metrics indicate 87.5% accuracy for the  $\pm\,10\,\%$  error band and 74 % for the  $\pm\,2\sigma$  confidence interval, with 100% sensitivity. Thereby, combining Groups I and II improves robustness.

## 3.3.3. Isobaric Correlation

To eliminate pressure influence, an isobaric correlation is performed using data at  $1.05\pm0.05\,\mathrm{MPa}$ . The 13 valid datasets are divided into three groups each containing four or five datasets. The mean deviations of predicted joint qualities are significantly below the experimental uncertainty range. Binary metrics show excellent predictive quality with 100% accuracy and precision for the  $\pm10\,\%$  error band

and values over 80% for the  $\pm 2\sigma$  confidence interval, confirming improved prediction quality when pressure dependency is minimised. These values align accurately with findings from [45] on Al-based quality prediction in ultrasonic welding.

### 3.4. Application Limits

Plotting the Sänger factors,  $\Theta_S$ , against the mechanical weld factors,  $\Theta_M$ , reveals a near-horizontal trend line in the correlation diagrams (Fig. 8). This indicates that  $\Theta_S$  remains almost constant despite process variations in  $\Theta_M$ , suggesting the model's limited sensitivity to pressure changes, which are not fully captured in the pure thermal-electric simulation. This hypothesis can be validated via Groups III and IV as their mechanical properties reflect pure pressure dependency. Their  $\Theta_S$  remains nearly constant across varying pressures, while  $\Theta_M$  fluctuates significantly.

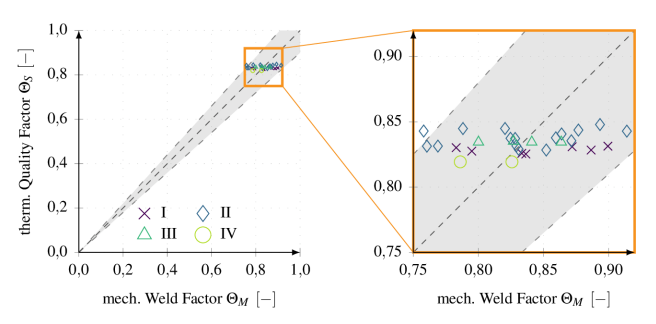


FIG 8. Correlation Diagram between Mechanical Weld Factors,  $\Theta_M$ , and Thermal Quality Factors,  $\Theta_S$  for the four investigation groups within the  $\pm$  10 % error band by [23]

The model's valid application range is thus limited to  $\Theta_M$  values around the mean value of  $\overline{\Theta}_M=0.834$  of the investigated dataset. Below this range, the model tends to overestimate joint quality, which is undesirable for predictive accuracy [90]. The overestimation is particularly evident for  $\Theta_M\lessapprox 0.75$ , often due to incomplete welding. To assess this, prematurely terminated welding processes are analysed which are halted before completion, resulting in mechanical weld factors,  $\Theta_M$ , ranging from 0.422 to 0.692. The corresponding calculated Sänger factors,  $\Theta_S$ , show significant overestimation of joint quality with values ranging from 0.824 to 0.836, aligning with observations by [43] for incomplete ultrasonic welding processes.

This discrepancy arises from deviations in the simulated heating behaviour compared to real tests. While simulations accurately match measured temperatures for complete processes, premature termination leads to higher simulated temperatures, causing overestimation of the melting degree,  $\psi_m$ , and thus  $\Theta_S$ . Taking an exemplary test series, its simulated temperature overestimates  $\psi_m$  as 1.000 instead of the actual 0.404 based on the real measured temperature, which would accurately predict its determined  $\Theta_M = 0.422$ .

### 4. CONCLUSION

# 4.1. Summary

7

Currently, the standard approach for developing new joining processes involves experimental sample production within a test pyramid, followed by mechanical testing. This sequential process is resource-intensive in terms of time, cost, and materials, often neglecting process alternatives and optimi-

©2025

TAB 5. Comparison of predictive quality across extrapolation scenarios

	MAE	$\overline{\Delta\Theta_M}$		±10%			$\pm 2\sigma$		
			acc	prec	rec	acc	prec	rec	
general	0,038	0,058	93,3 %	93,3%	100,0%	76,7%	83,3 %	93,3%	
special I	0,043	0,053	100,0%	100,0%	100,0%	61,1 %	77,8%	83,3%	
special II	0,041	0,059	87,5%	87,5%	100,0%	75,0%	75,0%	100,0%	
special I+II	0,043	0,057	87,5%	87,5%	100,0%	74,2%	79,2%	95,0%	
isobaric	0,035	0,067	100,0%	100,0%	100,0%	83,8 %	83,3 %	100,0%	

sation potential. It also offers limited scalability and future expandability of the certified process window.

The joining quality produced depends largely on the thermal history of the joining partners. This can be modelled very well using modern FEM process simulations, but to date it has hardly been used to predict the mechanical strength. The motivation behind this work is to close this gap and contribute to shorter development times with reduced use of resources while simultaneously increasing the degree of digitalisation in the research of new joining technologies.

This work investigated the hypothesis of a mechanical-thermal analogy to establish a correlation between measurable mechanical properties and a newly introduced thermally based quality factor, the Sänger factor. A model was developed to predict joint quality based on the simulated temperature state in the joining zone utilising four different temperature characteristics. The predictive capability of the model was evaluated across various study groups and joint quality with mechanical welding factors  $\gtrsim 0.75$  was predicted with good to very good agreement — peaking in the isobaric correlation achieving the highest accuracy.

# 4.2. Outlook

To enhance the reliability of predictions, several extensions are proposed. The isobaric correlation highlighted the negative impact of neglected pressure dependency. Future work should integrate mechanical degrees of freedom in simulations to account for pressure dependency, which significantly affects joint quality [96]. Additionally, incorporating pore formation models [97] and moisture effects [98,99] could enhance predictive accuracy. Expanding the mathematical formulation to include a consolidation model for "autohesion" [100, 101] would improve predictions for incomplete welds, while a continuous degradation model [102–104] could extend applicability to overheated samples. Refining the crystallisation model within FEM analysis [80, 81, 86] would further improve realism by coupling mechanical and thermal effects [105, 106].

The Sänger factor represents a valuable tool in the context of digitalisation, enabling virtual process optimisation, reducing experimental effort, and facilitating sustainable resource management in aerospace manufacturing. This thermally based quality factor approach is transferable to all thermoplastic welding processes, provided a process simulation exists to characterise heating and melting behaviour.

## **DECLARATIONS**

This work is a compendious reprint of the dissertation published in 2024 under the title "Ein Qualitätsfaktor beim Schweißen thermoplastischer Faserverbunde mittels Meso-Composite-Modell" [87].

### **Acknowledgements**

The author would like to thank the Center of Lightweight-Production-Technology (DLR-ZLP) for making the attendance and publication at the German Aerospace Congress 2025 possible.

#### **Conflict of Interest**

The author declared no potential conflicts of interest with respect to the research, authorship, and/or publication. of this article.

### **Funding**

The author disclosed receipt of the following financial support for the research, authorship, and/or publication of this article: This work was supported by the German Federal Ministry for Economic Affairs and Energy (BAnz AT 15.11.2019 B1) due to a decision of the German Bundestag under the grand number 20W1915A and the European Union Horizon 2020 Framework Programme (Grant agreement ID 945583).

# **Data Availability Statement**

Data sets generated during the current study are not openly available due to reasons of sensitivity and company secrest, but are available from the corresponding author upon reasonable request. Data are located in controlled access data storage of the affiliated company and/or institutes.

## **Al Usage Disclosure**

This document was created with assistance from AI tools. The content has been reviewed and edited by a human. For more information on the extent and nature of AI usage, please contact the author.

### ORCID ID

Alexander Sänger Oorcid.org/0009-0006-7734-5535

## **Contact address:**

alexander.saenger@airbus.com

### References

- [1] (Industrievereinigung Verstärkte Kunststoffe e.V.) AVK. Handbuch Faserverbundkunststoffe/Composites. Springer Fachmedien, 4 edition, 2014. ISBN: 978-3-658-02755-1.
- [2] C. Red. Thermoplastics in aerospace composites outlook, 2014-2023. 22(5), 2014. ISSN: 2376-5240.

- [3] S. Kothe, B. Diehl, D. Niermann, L. Chen, M. Wolf, and W. Hintze. Automated assembly of thermoplastic fuselage structures for future aircrafts. In B. Behrens, A. Brosius, W. Hintze, S. Ihlenfeldt, and J.P. Wulfsberg, editors, *Production at the leading edge of technology*, pages 467–475. Springer-Verlag, 2021. ISBN: 978-3-662-62138-7.
- [4] A. Strong. Fundamentals of Composites Manufacturing, Second Edition: Materials, Methods and Applications. Society of Manufacturing Engineers, 2008. ISBN: 978-0-872-63854-9.
- [5] S.L. Omairey, S. Sampethai, L. Hans, C. Worrall, S. Lewis, D. Negro, T. Sattar, E. Ferrera, E. Blanco, J. Wighton, L. Muijs, S.L. Veldman, M. Doldersum, R. Tonnaer, N. Jayasree, and M. Kazilas. Development of innovative automated solutions for the assembly of multifunctional thermoplastic composite fuselage. *The International Journal of Advanced Manufacturing Technology*, 117(5):1721–1738, 2021. ISSN: 1433-3015. DOI: 10.1007/s00170-021-07829-2.
- [6] A. Yousefpour, M. Hojjati, and J. Immarigeon. Fusion bonding/welding of thermoplastic composites. *Journal of Thermoplastic Composite Materials*, 17(4):303– 341, 2004. DOI: 10.1177/0892705704045187.
- [7] T. Ahmed. D. Stavrov. Н. Bersee. and A. Beukers. Induction welding of thermoplastic composites—an overview. Composites Part A: Applied Science and Manufacturing, 37(10):1638–1651, 2006. ISSN: 1359-835X. DOI: 10.1016/j.compositesa.2005.10.009.
- [8] A.P.d. Costa, E.C. Botelho, M.L. Costa, N.E. Narita, and J.R. Tarpani. A review of welding technologies for thermoplastic composites in aerospace applications. 4(3):255–265. ISSN: 0403-3912.
- [9] L. Larsen, Dominik Görick, M. Engelschall, F. Fischer, and M. Kupke. Process data driven advancement of robot-based continuous ultrasonic welding. In *Inter*national Conference and Exhibition on Thermoplastic Composites, 2020.
- [10] V.K. Stokes. Joining methods for plastics and plastic composites: An overview. *Polymer Engineering & Science*, 29(19):1310–1324, 1989. ISSN: 1548-2634. DOI: 10.1002/pen.760291903.
- [11] C. Ageorges, L. Ye, and M. Hou. Advances in fusion bonding techniques for joining thermoplastic matrix composites: a review. *Composites Part A: Applied Science and Manufacturing*, 32(6):839– 857, 2001. ISSN:1359-835X. DOI:10.1016/S1359-835X(00)00166-4.
- [12] I.F. Villegas, L. Moser, A. Yousefpour, P. Mitschang, and H.E. Bersee. Process and performance evaluation of ultrasonic, induction and resistance welding of advanced thermoplastic composites.
- [13] (Federal Aviaton Administration) FAA. Composite aircraft structure. Advisory Circular AC 20-107B, 2010.
- [14] X. Xiao, S. Hoa, and K. Street. Processing and modelling of resistance welding of apc-2 composite. *Jour*nal of Composite Materials, 26(7):1031–1049, 1992. DOI: 10.1177/002199839202600705.

- [15] H. Shi. Resistance welding of thermoplastic composites – process and performance. PhD thesis, 2014. DOI: 10.4233/uuid:58f16f99-afc1-4713-842e-562412583340.
- [16] Manuel Endraß, S. Jarka, S. Bauer, A. Huber, C. Stehncken, L. Larsen, and M. Kupke. Upscaling resistance welding - joining of carbon fiber composites for full-scale aerospace components. 2019.
- [17] J. Rouchon. Certification of large airplane composite structures, recent progress and new trends in compliance philosophy. In Congress of the International Council of the Aeronautical Sciences (ICAS Proceedings), volume 17, pages 1439–1447.
- [18] Y. Buchwald. Der virtuelle weg zur zulassung. (161):14–17, 2019. ISSN: 2190-0094.
- [19] F. Cianetti, G. Morettini, M. Palmieri, and G. Zucca. Virtual qualification of aircraft parts: test simulation or acceptable evidence? *Procedia Structural Integrity*, 24:526–540, 2019. ISSN: 2452-3216. AIAS 2019 International Conference on Stress Analysis. DOI: 10.1016/j.prostr.2020.02.047.
- [20] T.A. Laux. Experimental and computational characterisation of composite laminates subjected to multiaxial loading. PhD thesis, University of Southampton, 2020. https://eprints.soton.ac.uk/447127/.
- [21] Clean Sky 2. Prodige: Virtual certification methodologies are on the horizon.
- [22] T. Olbrechts. Virtual aircraft certification, where do we stand, where are we going?, 2023. https://www.linkedin.com/pulse/virtual-aircraft-certification-where-do-we-stand-going-olbrechts.
- [23] (European Union Aviation Safety Agency) EASA. Proposed certification memorandum on modelling & simulation cs-25 structural certification specifications. Certification Memoranda CM-S-014, 2020.
- [24] D. Stavrov and H. Bersee. Resistance welding of thermoplastic composites-an overview. Composites Part A: Applied Science and Manufacturing, 36(1):39–54, 2005. ISSN:1359-835X. DOI: 10.1016/j.compositesa.2004.06.030.
- [25] P. Mitschang, R. Rudolf, and M. Neitzel. Continuous induction welding process, modelling and realisation. *Journal of Thermoplastic Composite Materials*, 15(2):127–153, 2002. DOI: 10.1177/0892705702015002451.
- [26] X. Wang, J. Yan, R. Li, and S. Yang. Fem investigation of the temperature field of energy director during ultrasonic welding of peek composites. *Journal of Thermoplastic Composite Materials*, 19(5):593–607, 2006. DOI: 10.1177/0892705706067479.
- [27] A. Levy, S. Le Corre, and I. Villegas. Modeling of the heating phenomena in ultrasonic welding of thermoplastic composites with flat energy directors. *Journal of Materials Processing Technology*, 214(7):1361–71, 2014. ISSN:0924-0136. DOI:10.1016/j.jmatprotec.2014.02.009.

©2025

9

- [28] S. Tutunjian, M. Dannemann, N. Modler, M. Kucher, and A. Fellermayer. A numerical analysis of the temporal and spatial temperature development during the ultrasonic spot welding of fibre-reinforced thermoplastics. *Journal of Manufacturing and Materials Processing*, 4(2), 2020. ISSN: 2504-4494. DOI: 10.3390/jmmp4020030.
- [29] J. Koyanagi, M. Takamura, K. Wakayama, K. Uehara, and S. Takeda. Numerical simulation of ultrasonic welding for cfrp using energy director. *Advanced Composite Materials*, 31(4):428–441, 2022. DOI: 10.1080/09243046.2022.2031376.
- [30] A. Maffezzoli, J. Kenny, and L. Nicolais. Welding of peek/carbon fiber composite laminates. SAMPE Journal, 25(1):35–40, 1989.
- [31] T.B. Jakobsen, R.C. Don, and J.W. Gillespie. Twodimensional thermal analysis of resistance welded thermoplastic composites. *Polymer Engineering & Science*, 29(23):1722–1729, 1989. ISSN: 1548-2634. DOI: 10.1002/pen.760292314.
- [32] S.T. Holmes and J.W. Gillespie. Thermal analysis for resistance welding of large-scale thermoplastic composite joints. *Journal of Reinforced Plastics and Composites*, 12(6):723–736, 1993. DOI:10.1177/073168449301200609.
- [33] C. Ageorges, L. Ye, Y. Mai, and M. Hou. Characteristics of resistance welding of lap shear coupons. part i: Heat transfer. *Composites Part A: Applied Science and Manufacturing*, 29(8):899–909, 1998. ISSN: 1359-835X. DOI: 10.1016/S1359-835X(98)00022-0.
- [34] R. Carbone and A. Langella. Numerical modeling of resistance welding process in joining of thermoplastic composite materials using comsol multiphysics. In *Proceedings of the COMSOL Conference 2009*, 2009.
- [35] H. Shi, I. Villegas, and H. Bersee. Modelling of heat transfer and consolidation for thermoplstic composites resistance welding. 2011.
- [36] H. Shi, I.F. Villegas, M. Octeau, H.E. Bersee, and A. Yousefpour. Continuous resistance welding of thermoplastic composites: Modelling of heat generation and heat transfer. Composites Part A: Applied Science and Manufacturing, 70:16–26, 2015. ISSN: 1359-835X. DOI: 10.1016/j.compositesa.2014.12.007.
- [37] É. Talbot, P. Hubert, M. Dubé, and A. Yousefpour. Optimization of thermoplastic composites resistance welding parameters based on transient heat transfer finite element modeling. *Journal of Thermoplastic Composite Materials*, 26(5):699–717, 2013. DOI:10.1177/0892705711428657.
- [38] F. Lionetto, S. Pappadà, G. Buccoliero, and A. Maffezzoli. Finite element modeling of continuous induction welding of thermoplastic matrix composites. *Materials & Design*, 120:212 221, 2017. ISSN: 0264-1275. DOI: 10.1016/j.matdes.2017.02.024.
- [39] Z.S. Colak, F.O. Sonmez, and V. Kalenderoglu. Process modeling and optimization of resistance welding for thermoplastic composites. *Journal*

- of Composite Materials, 36(6):721–744, 2002. DOI: 10.1177/0021998302036006507.
- [40] A. Benatar and T.G. Gutowski. Ultrasonic welding of peek graphite apc-2 composites. *Polymer Engineer*ing & Science, 29(23):1705–1721, 1989. ISSN: 1548-2634. DOI: 10.1002/pen.760292313.
- [41] Y. Li, T.H. Lee, C. Wang, K. Wang, C. Tan, M. Banu, and S.J. Hu. An artificial neural network model for predicting joint performance in ultrasonic welding of composites. *Procedia CIRP*, 76:85–88, 2018. ISSN: 2212-8271. 7th CIRP Conference on Assembly Technologies and Systems (CATS 2018). DOI: 10.1016/j.procir.2018.01.010.
- [42] Y. Li, Z. Liu, J. Shen, T.H. Lee, M. Banu, and S.J. Hu. Weld quality prediction in ultrasonic welding of carbon fiber composite based on an ultrasonic wave transmission model. *Journal of Manufacturing Science* and Engineering, 141(8):081010, 2019. ISSN: 1087-1357. DOI: 10.1115/1.4043900.
- [43] Y. Li, T.H. Lee, M. Banu, and S.J. Hu. An integrated process-performance model of ultrasonic composite welding based on finite element and artificial neural network. *Journal of Manufacturing Processes*, 56:1374–1380, 2020. ISSN: 1526-6125. DOI: 10.1016/j.jmapro.2020.04.033.
- [44] Y. Li, B. Yu, B. Wang, T.H. Lee, and M. Banu. Online quality inspection of ultrasonic composite welding by combining artificial intelligence technologies with welding process signatures. *Materials & Design*, 194:108912, 2020. ISSN: 0264-1275. DOI: 10.1016/j.matdes.2020.108912.
- [45] D. Görick, L. Larsen, M. Engelschall, and A. Schuster. Quality prediction of continuous ultrasonic welded seams of high-performance thermoplastic composites by means of artificial intelligence. *Procedia Manufacturing*, 55:116–123, 2021. ISSN: 2351-9789. FAIM 2021. DOI: 10.1016/j.promfg.2021.10.017.
- [46] E. Doege and B. Behrens. Handbuch Umformtechnik: Grundlagen, Technologien, Maschinen. VDI-Buch. Springer-Verlag, 2016. ISBN: 978-3-662-43890-9.
- [47] H. Haberhauer and F. Bodenstein. *Maschinenelemente: Gestaltung, Berechnung, Anwendung.*Springer-Lehrbuch. Springer-Verlag, 2018. ISBN: 978-3-662-53047-4.
- [48] K. Wang, D. Shriver, M. Banu, S. Jack Hu, G. Xiao, J. Arinez, and H. Fan. Performance prediction for ultrasonic spot welds of short carbon fiber-reinforced composites under shear loading. *Journal of Manufacturing Science and Engineering*, 139(11), 2017. ISSN:1087-1357. 111001. DOI:10.1115/1.4037320.
- [49] B.A. Bednarcyk, B. Stier, J. Simon, S. Reese, and E.J. Pineda. Meso- and micro-scale modeling of damage in plain weave composites. *Composite Structures*, 121:258–270, 2015. ISSN: 0263-8223. DOI: 10.1016/j.compstruct.2014.11.013.
- [50] S. Yu, D. Zhang, and K. Qian. Numerical analysis of macro-scale mechanical behaviors of 3d orthogonal woven composites using a voxel-based finite element model. *Applied Composite Materials*, 26(1):65–83,

- 2019. ISSN: 1573-4897. DOI: 10.1007/s10443-018-9707-z.
- [51] L. Girdauskaite, G. Haasemann, and S. Krzywinski. Modellierung und Simulation, chapter 15. Springer-Verlag. ISBN: 978-3-642-17991-4.
- [52] L. Nagel, A. Herwig, C. Schmidt, and P. Horst. Numerical investigation of residual stresses in welded thermoplastic cfrp structures. *Journal of Composites Science*, 5(2), 2021. ISSN: 2504-477X. DOI: 10.3390/jcs5020045.
- [53] H. Shi, I. Villegas, and H. Bersee. An investigation on the strain distribution of resistance welded thermoplastic composite joints. 2012. DOI: 10.2514/6.2012-1448.
- [54] M. Neitzel, P. Mitschang, and U. Breuer. Handbuch Verbundwerkstoffe. Carl Hanser Verlag GmbH & Co. KG, 2 edition, 2014. ISBN: 978-3-446-43697-8.
- [55] J. Rotheiser. Joining of Plastics: Handbook for Designers and Engineers. Hanser Publishers, 2004. ISBN: 978-1-569-90354-4.
- [56] S. Thissen and Manuel Endraß.
- [57] T. Ishikawa. Anti-symmetric elastic properties of composite plates of satin weave cloth. Fibre Science and Technology, 15(2):127–145, 1981. ISSN: 0015-0568. DOI: 10.1016/0015-0568(81)90066-X.
- [58] T. Ishikawa and T. Chou. Elastic behavior of woven hybrid composites. *Journal of Composite Materials*, 16(1):2–19, 1982. DOI: 10.1177/002199838201600101.
- [59] T.C. Ishikawa. Stiffness and strength behaviour of woven fabric composites. *Journal of Materials Science*, 17(11):3211–3220, 1982. ISSN: 1573-4803. DOI: 10.1007/BF01203485.
- [60] T. Ishikawa and T. Chou. One-dimensional micromechanical analysis of woven fabric composites. AIAA Journal, 21(12):1714–1721, 1983. DOI: 10.2514/3.8314.
- [61] C. Ageorges, L. Ye, and M. Hou. Experimental investigation of the resistance welding of thermoplastic-matrix composites. part ii: optimum processing window and mechanical performance. *Composites Science and Technology*, 60(8):1191–1202, 2000. ISSN: 0266-3538. DOI: 10.1016/S0266-3538(00)00025-7.
- [62] DIN EN 2243-1. Prüfverfahren teil 1: Bestimmung der bindefestigkeit von einschnittig überlappten klebungen im zugversuch.
- [63] M. Hou and K. Friedrich. Resistance welding of continuous glass fibre-reinforced polypropylene composites. *Composites Manufacturing*, 3(3):153– 163, 1992. ISSN:0956-7143. DOI:10.1016/0956-7143(92)90078-9.
- [64] M. Singh and H. Kaur. Artificial neural networks in material science research. Current Reports on Science and Technology, 2:145–159, 2016.

- [65] C. Ageorges, L. Ye, Y. Mai, and M. Hou. Characteristics of resistance welding of lap shear coupons. part ii: Consolidation. Composites Part A: Applied Science and Manufacturing, 29(8):911–919, 1998. ISSN:1359-835X. DOI:10.1016/S1359-835X(98)00023-2.
- [66] G. Ehrenstein, G. Riedel, and P. Trawiel. Thermal Analysis of Plastics. Hanser, 2004. ISBN: 978-1-569-90362-9.
- [67] H. Schürmann. Konstruieren mit Faser-Kunststoff-Verbunden. VDI-Buch. Springer-Verlag, 2 edition, 2007. ISBN: 978-3-540-72190-1.
- [68] A. Frick and C. Stern. Einführung in die Kunststoffprüfung: Prüfmethoden und Anwendungen. Carl Hanser Verlag GmbH & Co. KG, 2017. ISBN: 978-3-446-44988-6.
- [69] W. Kaiser. Kunststoffchemie für Ingenieure: Von der Synthese bis zur Anwendung. Carl Hanser Verlag GmbH & Co. KG, 2015. ISBN: 978-3-446-44774-5.
- [70] C. Hopmann and W. Michaeli. Einführung in die Kunststoffverarbeitung. Carl Hanser Verlag GmbH & Co. KG, 2017. ISBN: 978-3-446-45356-2.
- [71] M. Bradley. Void modeling in resin infusion, 2015. ht tp://hdl.lib.byu.edu/1877/etd8662.
- [72] S.H. McKnight, S.T. Holmes, J.W. Gillespie, C.L.T. Lambing, and J.M. Marinelli. Scaling issues in resistance-welded thermoplastic composite joints. Advances in Polymer Technology, 16(4):279–295, 1997. DOI:10.1002/(SICI)1098-2329(199711)16:4<279::AID-ADV3>3.0.CO;2-S.
- [73] C. Ageorges, L. Ye, and M. Hou. Experimental investigation of the resistance welding for thermoplastic-matrix composites. part i: heating element and heat transfer. *Composites Science and Technology*, 60(7):1027 1039, 2000. ISSN:0266-3538. DOI:10.1016/S0266-3538(00)00005-1.
- [74] A.G. Medea. Determination of the homogeneity of an image, 2019. https://www.medealab.de/en/2019/07 /10/homogeneity-image-processing/.
- [75] U. Knauer and B. Meffert. Fast computation of region homogeneity with application in a surveillance task. volume XXXVIII, pages 337–342. International Archives of Photogrammetry, Remote Sensing and Spatial Information Sciences.
- [76] M.F. Talbott, G.S. Springer, and L.A. Berglund. The effects of crystallinity on the mechanical properties of peek polymer and graphite fiber reinforced peek. *Journal of Composite Materials*, 21(11):1056–1081, 1987. DOI: 10.1177/002199838702101104.
- [77] W.I. Lee, M.F. Talbott, G.S. Springer, and L.A. Berglund. Effects of cooling rate on the crystallinity and mechanical properties of thermoplastic composites. *Journal of Reinforced Plastics and Composites*, 6(1):2–12, 1987. DOI: 10.1177/073168448700600101.

- [78] N. Batista, P. Olivier, G. Bernhart, M. Rezende, and E. Botelho. Correlation between degree of crystallinity, morphology and mechanical properties of pps/carbon fiber laminates. *Materials Research*, 19(1):195–201, 2016. DOI: 10.1590/1980-5373-MR-2015-0453.
- [79] G. Habenicht. Kleben: Grundlagen, Technologien, Anwendungen. VDI-Buch. Springer, 2008. ISBN: 978-3-540-85264-3.
- [80] C. Ageorges, L. Ye, Y. Mai, and M. Hou. Characteristics of resistance welding of lap-shear coupons. part iii: Crystallinity. Composites Part A: Applied Science and Manufacturing, 29(8):921–932, 1998. ISSN:1359-835X. DOI:10.1016/S1359-835X(98)00024-4.
- [81] C. Freist. Experimentelle und numerische Untersuchungen zum Widerstandsschweißen endlosfaserund kurzfaserverstärkter thermoplastischer Hochleistungsstrukturen. PhD thesis.
- [82] Thomas Guglhör. Experimentelle und modellhafte Betrachtung des Konsolidierungsprozesses von carbonfaserverstärktem Polyamid-6. Doktorarbeit, Universität Augsburg, 2017.
- [83] H. Domininghaus. Kunststoffe. VDI-Buch. Springer-Verlag, 2013. ISBN: 978-3-642-16173-5.
- [84] J. Sierra, M. Noriega Escobar, J. Gómez, and J. Pastor. Isothermal and non-isothermal crystallization kinetics for blends of polyamide 6 and polypropylene. Zeitschrift Kunststofftechnik/Journal of Plastics Technology, 2006.
- [85] Simutence. Kristallisationskinetik pps. 2019.
- [86] P. Sekol. Entwicklung und implementierung eines kristallisationsmodells für ein thermoplast-schweißverfahren.
- [87] Alexander Sänger. Ein Qualitätsfaktor beim Schweisen thermoplastischer Faserverbunde mittels Meso-Composite-Modell. doctoralthesis, Universität Augsburg, 2024.
- [88] K. Choo, E. Greplova, M. Fischer, and T. Neupert. Machine Learning kompakt: Ein Einstieg für Studierende der Naturwissenschaften. essentials. Springer Fachmedien Wiesbaden, 2021. ISBN: 978-3-658-32267-0.
- [89] B. Botsch. Maschinelles Lernen Grundlagen und Anwendungen: Mit Beispielen in Python. Springer Berlin, 2023. ISBN: 978-3-662-67276-1.
- [90] P. Safarian. Finite element modeling and analysis validation. https://appliedcax.com/docs/femap/femap-symposium-2015-seattle-area/FEA-Validation-Requiremnents-and-Methods-Final-with-Transcript.pdf.
- [91] M. Plaue. *Data Science: Grundlagen, Statistik und maschinelles Lernen*. Springer-Verlag, 2021. ISBN: 978-3-662-63488-2.
- [92] R. Micheloni and C. Zambelli. Machine Learning and Non-volatile Memories. Springer International Publishing, 2022. ISBN: 978-3-031-03841-9.

- [93] C. Hsu, C. Chang, and C. Lin. A practical guide to support vector classification. Technical report, 2016.
- [94] R. Bellman. Adaptive Control Processes: A Guided Tour. Princeton University Press, 1961. ISBN: 978-1-400-87466-8.
- [95] F. Chollet. Deep Learning mit Python und Keras: Das Praxis-Handbuch vom Entwickler der Keras-Bibliothek. mitp Professional. MITP, 2018. ISBN: 978-3-958-45840-6.
- [96] H. Shi, I.F. Villegas, and H.E. Bersee. Analysis of void formation in thermoplastic composites during resistance welding. *Journal of Thermoplastic Composite Materials*, 30(12):1654–1674, 2017. DOI:10.1177/0892705716662514.
- [97] R. Pitchumani, S. Ranganathan, R. Don, J. Gille-spie, and M. Lamontia. Analysis of transport phenomena governing interfacial bonding and void dynamics during thermoplastic tow-placement. *International Journal of Heat and Mass Transfer*, 39(9):1883–1897, 1996. ISSN: 0017-9310. DOI: 10.1016/0017-9310(95)00271-5.
- [98] J.L. Kardos, M. P. Duduković, and R. Dave. Void growth and resin transport during processing of thermosetting — matrix composites. In K. Dušek, editor, *Epoxy Resins and Composites IV*, pages 101–123. Springer-Verlag, 1986. ISBN: 978-3-540-39775-5.
- [99] J. Anderson and M. Altan. Formation of voids in composite laminates: Coupled effect of moisture content and processing pressure. *Polymer Composites*, 36(2):376–384, 2015. DOI: 10.1002/pc.22952.
- [100] Y.H. Kim and R.P. Wool. A theory of healing at a polymer-polymer interface. *Macromolecules*, 16(7):1115–1120, 1983. ISSN: 0024-9297. DOI: 10.1021/ma00241a013.
- [101] R.P. Wool and K.M. O'Connor. A theory crack healing in polymers. *Journal of Applied Physics*, 52(10):5953–5963, 1981. ISSN: 0021-8979. DOI: 10.1063/1.328526.
- [102] R. Pitchumani, J.W. Gillespie, and M.A. Lamontia. Design and optimization of a thermoplastic tow-placement process with in-situ consolidation. *Journal of Composite Materials*, 31(3):244–275, 1997. DOI: 10.1177/002199839703100302.
- [103] H. Farong, W. Xueqiu, and L. Shijin. The thermal stability of polyetherimide. *Polymer Degradation and Stability*, 18(3):247–259, 1987. ISSN: 0141-3910. DOI: 10.1016/0141-3910(87)90005-X.
- [104] J. Nam and J.C. Seferis. Generalized composite degradation kinetics for polymeric systems under isothermal and nonisothermal conditions. *Journal of Polymer Science Part B: Polymer Physics*, 30(5):455–463, 1992. DOI: 10.1002/polb.1992.090300505.
- [105] M. Moneke. Die Kristallisation von verstärkten Thermoplasten während der schnellen Abkühlung und unter Druck. PhD thesis, Technische Universität Darmstadt, 2001. http://tuprints.ulb.tu-darmstadt .de/155/.

[106] G. Menges, E. Haberstroh, W. Michaeli, and E. Schmachtenberg. *Menges Werkstoffkunde Kunst-stoffe*. Carl Hanser Verlag GmbH & Co. KG, 2014. ISBN: 978-3-446-44353-2.